

## Entanglement of Optical and Microcavity Modes by Means of an Optoelectronic System

Ahmad Salmanoglu,<sup>1,2,\*</sup> Dincer Gokcen,<sup>2</sup> and H. Selcuk Gecim<sup>1</sup>

<sup>1</sup>*Faculty of Engineering, Electrical and Electronics Engineering Department, Çankaya University, Ankara, Turkey*

<sup>2</sup>*Faculty of Engineering, Electrical and Electronics Engineering Department, Hacettepe University, Ankara, Turkey*



(Received 18 June 2018; revised manuscript received 13 December 2018; published 28 February 2019)

Entanglement between optical and microwave cavity modes is a critical issue in illumination systems. Optomechanical systems are utilized to introduce coupling between the optical and microwave cavity modes. However, due to some restrictions of the optomechanical system, especially sensitivity to the thermal photon noise at room temperature, an alternative optoelectronic system is designed to address the problem. We study a method by which it may be possible to remove the mechanical part of the previous systems to minimize the thermally generated photons. Unlike optomechanical systems, in our system, the optical mode is directly coupled to the microwave cavity mode through the optoelectronic elements without employing any mechanical parts. The utilized approach leads to generating the entangled modes at room temperature. For this purpose, the dynamics of the motion of the optoelectronic system is theoretically derived using the Heisenberg-Langevin equations from which one can calculate the coupling between optical and microwave cavity modes. The direct coupling between the optical and microwave cavity modes is the most important feature and is achieved through the combination of the photodetector and a Varactor diode. Hence, by controlling the photodetector current, that is, the photocurrent, depending on the optical cavity incident wave and the Varactor diode-biased voltage, the coupling between the optical and microwave cavity modes is established. The voltage across the Varactor diode also depends on the generated photocurrent. Consequently, our results show that the coupled modes are entangled at room temperature without the requirement for any mechanical parts.

DOI: 10.1103/PhysRevApplied.11.024075

### I. INTRODUCTION

In recent years, fabrication of sensitive sensors has been a subject of intensive research. Undoubtedly, this technological trend will replace classical sensors with quantum sensors because quantum-based sensors are able to provide some important advantages to improve the sensor's performance such as resolution enhancement [1,2] in quantum imaging, sensitivity improvement [3,4] in quantum radar, and so on. Indeed, the nonclassical and entanglement methods utilized in quantum-based sensors are produced in various approaches [5–7]. These alternative phenomena improve the sensor performance in different applications such as plasmonics [8,9], Raman spectroscopy [10], and others. By definition, entanglement is established when two photons are generated to interact in such a way that their properties are linked to each other [11,12]. It is significant to note that the link between the related photons or states is nonclassical. In entangled photons, determining the position, momentum, spin, or polarization of one

photon does not depend on the interdistance between the photons. This allows examination of the complementary position, momentum, spin, or polarization of the partner photon at that distinct point [3]. To date, this unique quantum property has been widely used in different applications to improve system specifications. One of the important systems, that is, quantum illumination, utilizes the entanglement to enhance features such as sensitivity and signal-to-noise ratio [3,4]. The illumination systems especially produce the entangled modes between the optical cavity (OC) and microwave (MW) cavity modes. The optomechanical subsystem is mostly employed to produce the entangled modes [13–17]. One of the critical problems of the illumination systems that utilize a mechanical part involves the thermal photons induced, which restrict the system operation at high temperatures. This problem is basically induced because the mechanical part operates at a low frequency compared to the OC and MW cavity frequencies. Consequently, the thermal photons generated in the mechanical subsystem limit the system's operation. However, in order to address the problem mentioned above, some works have been reported on bandwidth

\*tirdad.zey@gmail.com

engineering [14–16]. Furthermore, in our previous work [17], an alternative system was designed based on the plasmonic effect where the plasmon–plasmon interaction was utilized to modify the total capacitance. As a result, entanglement at high operational temperatures (100–150 K) was achieved. Both bandwidth engineering and manipulating the optical cavity modes through the plasmonic effect may restrict the generation of thermally induced photons. Nonetheless, the number of thermal photons generated at room temperature is so high that it confines the cavity modes’ entangling in conventional systems. As mentioned before, there are some critical problems with employing mechanical parts in the illumination systems. In fact, operation of the mechanical components at low frequency induces the generation of thermal photons, which is the main source of the noise that strongly affects the entanglement between OC and MW cavity modes, especially at room temperature. Another important point is that in the classical tripartite systems [13–17], the OC modes cannot directly couple to the MW cavity modes. As a matter of fact, the optical mode has to initially couple to the mechanical mode, and then this mode will couple to the microcavity mode. In some reported work [14–16], the unwanted influence of the mechanical unit on the output modes has been partially suppressed. In fact, the problem is that the unwanted effect induced by the mechanical unit can strongly influence the entanglement between the OC and MW modes [15,17]. In light of the information discussed above, the main idea of this study is that bypassing the mechanical unit strongly helps to eliminate the generation of thermal photons, thus the resulting entanglement between the OC and MW cavity modes is not affected by the extra thermal photons. Therefore, the mechanical parts are completely removed in this design to minimize the related noise. By utilization of the optoelectronic subsystem, the OC modes are directly coupled to the MW cavity modes without any mechanical unit. It is shown that bypassing the mechanical unit and utilizing the optoelectronic unit causes a dramatic decrease in the generation of thermal photons. With this method, the entanglement between the OC and MW cavity modes is strongly enhanced.

In this work, the OC modes are initially coupled to a photodetector, leading to photocurrent generation in the near-infrared (NIR) [18–20]. Then the coupling between the OC and MW cavity modes is established by voltage developed across the Varactor diode [21], which induces the photocurrent. The Varactor diode capacitance varies as a function of the applied voltage. As a result, the resonance frequency of the inductor-capacitor ( $LC$ ) circuit is expressed as a function of the Varactor diode capacitance. In fact, we theoretically prove and illustrate that using an optoelectronic system enables the cavity modes to remain entangled even at room temperature, since the effect of the thermal photons generated into the system

is reduced. Eventually, using the optoelectronic subsystem decreases the complexity of the illumination system and creates a certain degree of freedom for engineering the entanglement of the cavity modes.

## II. THEORY AND BACKGROUNDS

### A. System description

The proposed optoelectronic system illustrated in Fig. 1 shows the system design, which consists of an optical cavity, a photodetector, a Varactor diode, and an inductor. In this system, the optical cavity mode is initially coupled to the photodetector to generate a photocurrent, which is dependent on the incident light  $i = f_1(\omega)$ , where  $f_1$  stands for the coupling factor function. The photocurrent flows through the Varactor diode, resulting in the variation of the capacitance  $C = f_2(\omega)$ , where  $f_2$  is the other coupling factor. Consequently, the resonance frequency of the MW cavity is strongly related to the Varactor diode capacitor, which is a function of the photocurrent. In other words, it should be noted that such an optoelectronic design enables a direct coupling between the OC and the MW cavity modes. Additionally, a typical photodetector with its related responsivity is illustrated in Fig. 1(b). As shown in Fig. 1(c), a typical model of the Varactor diode is employed and the change of capacitance is shown as a function of the applied voltage. The models in Fig. 1(b) and Fig. 1(c) are only used to demonstrate the photodetector’s responsivity and the Varactor diode’s response, respectively. Figure 1(d) depicts the coupling of the OC to the photodetector, the photocurrent’s effect on the Varactor diode capacitance, and the influence of the OC mode on the MW cavity mode.  $A_\omega$  and  $\omega_\omega$  in Fig. 1(d) indicate the MW cavity mode amplitude and frequency, respectively. Furthermore,  $\omega_c$  stands for the OC mode frequency and  $A_c$  indicates its amplitude. It is important to emphasize that the coupling between the two cavity modes will be established by adjusting  $f_1$  and  $f_2$ . The ratio of  $f_1/f_2$  defines the effect of the OC mode on the MW cavity mode. As a result, by modifying the mentioned ratio, the entanglement between the cavity modes can be achieved even at room temperature.

### B. Optoelectronic system dynamics of motions

The total Hamiltonian [13,17] of the illustrated optoelectronic system in Fig. 1(a) is defined as

$$H_{\text{total}} = \frac{\varphi^2}{2L} + \frac{Q^2}{2C} - e(t)Q + \hbar\omega_c a^\dagger a - \hbar G_{\text{OC}} a^\dagger a \\ + i\hbar E_c (a^\dagger e^{(-j\omega_{\text{OC}} t)} - a e^{(j\omega_{\text{OC}} t)}), \quad (1)$$

where  $(\varphi, Q)$  are the canonical coordinates for the MW cavity and  $\varphi$ ,  $L$ , and  $Q$  are the inductor flux, inductance, and charge on capacitor  $C$ , respectively. Also,  $a$ ,  $a^\dagger$ ,  $\omega_{\text{OC}}$ ,

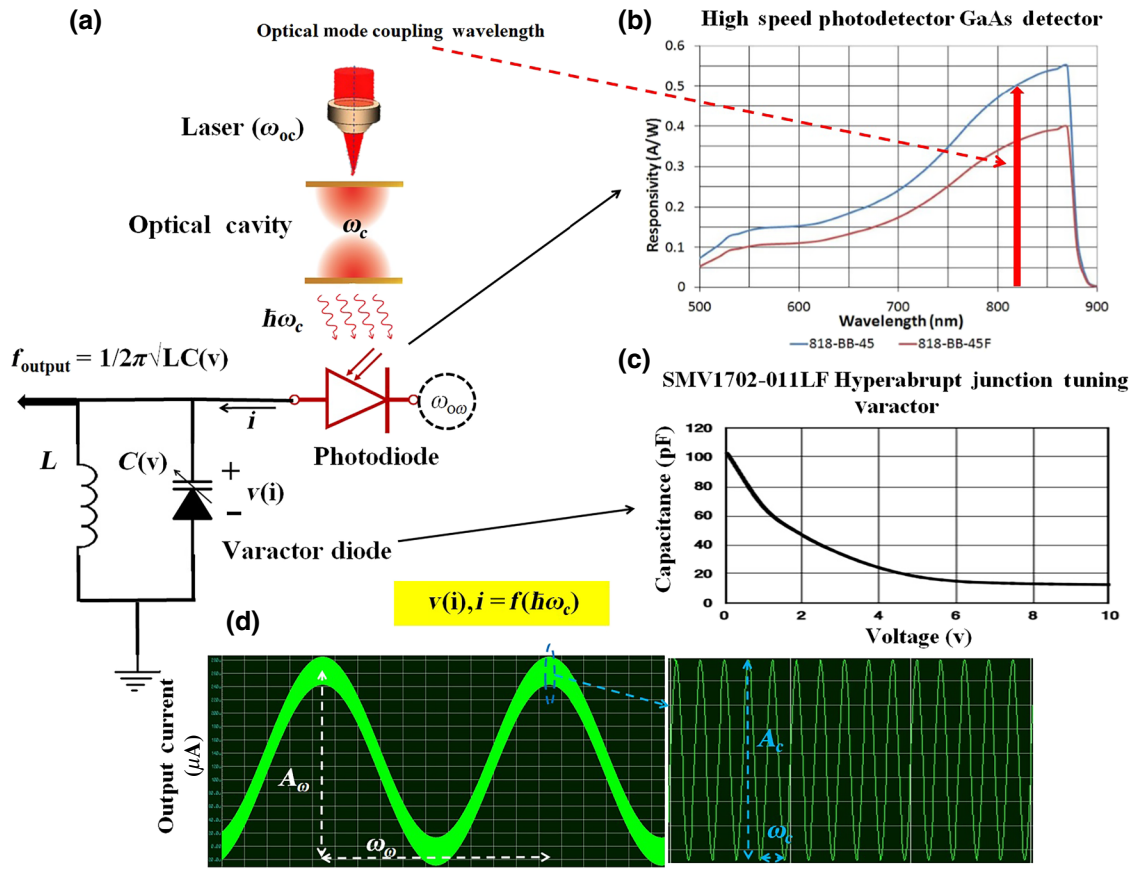


FIG. 1. Optoelectronic system schematic. (a) OC mode coupling to MW cavity mode through the photodetector and a Varactor diode; (b) a typical GaAs photodetector responsivity graph [22]; (c) Varactor diode capacitance variation vs biased voltage, which is the function of photodetector current [23]; (d) simulated photocurrent as a function of optical cavity mode incidence wave frequency and amplitude. The optical mode center wavelength is around 808 nm.

$E_c$ ,  $e(t)$ , and  $G_{OC}$  are the annihilation and creation operators of the optical cavity, the OC pump frequency, the OC input driving field, the MW cavity driving, and the coupling factor between the OC and MW modes, respectively.  $G_{OC}$  is a nonlinear function of  $f_1$  and  $f_2$  that indicates: (1) coupling between the OC and photodetector leading to the photocurrent flowing as a function of the incoming photons; (2) coupling between the photodetector and Varactor diode resulting in a varying capacitance of the Varactor diode, which then leads to monitoring the MW cavity modes.

By defining the lowering and raising operators for the MW cavity and by surpassing the fast oscillating frequencies, the system's total Hamiltonian is introduced as

$$H_{total} = \hbar\Delta_\omega b^+b + \hbar\Delta_c a^+a - \hbar q_{OC} a^+ab^+b \\ + i\hbar E_c(a^+ - a) + i\hbar E_\omega(b^+ - b), \quad (2)$$

where  $\Delta_\omega = \omega_\omega - \omega_{0\omega}$ ,  $\Delta_c = \omega_c - \omega_{0c}$ , and  $q_{OC}$  is proportional to  $G_{OC}$  depending on the MW cavity photons. The third

term,  $q_{OC}a^+ab^+b$ , in Eq. (2) defines the interaction Hamiltonian. This term specifically defines the degree of the interaction of the OC mode with the photodetector. In addition, through a nonlinear process controlled by  $q_{OC}$ , the contributed OC photons are converted to the MW cavity photons. It should be noted that Eq. (2) is derived using the canonical conjugation method [24] in which the matter is considered by a harmonic polarization field. In this study, the Varactor diode capacitor and inductance form the MW mode, which is basically established from the harmonic polarization field of their materials. It is emphasized that the disadvantage of this study seems to be that the Varactor diode is a macroscopic device whose operation is based on the interaction of a large number of charged particles. It can consequently affect the coherent function, especially at room temperature, which is due to the generation of the thermal photons. However, this contradiction is not observed in this design because of the following reasons: (1) the Varactor diode is utilized in this work since it has been proved that the capacitance and inductor in a MW circuit can conserve energy in a coherent

fashion at high temperature [15,16] and (2) the Varactor diode operation frequency is in the range of GHz, so the density of the induced thermal photons is negligibly small.

However, the dynamics of the OC and MW cavity modes in this system is also affected by the damping rate and noise operators such as thermal noise, quantum noise, and 1/f noise [25,26] since each mode interacts with its own environment. The equations of motions of this study employing the Heisenberg-Langevin equation are introduced as

$$\begin{aligned}\dot{a} &= -(i\Delta_c + \kappa_c)a + iq_{OC}ab^+ + E_c + \sqrt{2\kappa_c}a_{in}, \\ \dot{b} &= -(i\Delta_\omega + \kappa_\omega)b + iq_{OC}ba^+ + E_\omega + \sqrt{2\kappa_\omega}b_{in},\end{aligned}\quad (3)$$

where  $a_{in}$  and  $b_{in}$  are the OC cavity input noise and MW cavity input noise, respectively.  $\kappa_c$  and  $\kappa_\omega$  indicate the OC and MW cavity decay rates, respectively. In order to linearize Eq. (3), one can use the fluctuations associated with the field modes as  $q = \langle q \rangle + \delta q$ , where  $\langle q \rangle$  is the field average in the steady-state condition and  $\delta q$  indicates the fluctuation of the considered mode [14,17]. The linearization approach is justified because only the fluctuations, known as the noise around  $\langle q \rangle$ , are linearized, not the system itself.

Linearization of the noise for this system can be performed when the noise is small. Thus, it is possible to obtain the equations of motions based on the fluctuation

$$\begin{bmatrix} \dot{\delta a} \\ \dot{\delta a}^+ \\ \dot{\delta b} \\ \dot{\delta b}^+ \end{bmatrix} = \underbrace{\begin{bmatrix} -\gamma_c + iq_{OC}|\beta|^2 & 0 & i\alpha\beta q_{OC} & i\alpha\beta^* q_{OC}^* \\ 0 & -\gamma_c^* - iq_{OC}^*|\beta|^2 & -i\alpha^*\beta^* q_{OC}^* & -i\alpha^*\beta q_{OC} \\ i\alpha^*\beta q_{OC} & i\alpha\beta q_{OC} & -\gamma_\omega + iq_{OC}|\alpha|^2 & 0 \\ -i\alpha^*\beta^* q_{OC}^* & -i\alpha\beta^* q_{OC}^* & 0 & -\gamma_\omega^* - iq_{OC}^*|\alpha|^2 \end{bmatrix}}_{A_{ij}} \times \underbrace{\begin{bmatrix} \delta a \\ \delta a^+ \\ \delta b \\ \delta b^+ \end{bmatrix}}_{u(t)} + \underbrace{\begin{bmatrix} \sqrt{2\kappa_c}\delta a_{in} \\ \sqrt{2\kappa_c}\delta a_{in}^+ \\ \sqrt{2\kappa_\omega}\delta b_{in} \\ \sqrt{2\kappa_\omega}\delta b_{in}^+ \end{bmatrix}}_{n(t)}, \quad (7)$$

where  $\gamma_c = \kappa_c + i\Delta_c$  and  $\gamma_\omega = \kappa_\omega + i\Delta_\omega$ . Equation (7) yields  $u(t) = \exp(A_{ij}t)u(0) + \int [\exp(A_{ij}s)n(t-s)]ds$ , where  $n(s)$  is the noise column matrix. The related input noises obey the following correlation function [9–11]

$$\begin{aligned}\langle a_{in}(s)a_{in}^*(s') \rangle &= [N(\omega_c) + 1]\delta(s-s'); \quad \langle a_{in}^*(s)a_{in}(s') \rangle \\ &= [N(\omega_c)]\delta(s-s'), \\ \langle b_{in}(s)b_{in}^*(s') \rangle &= [N(\omega_\omega) + 1]\delta(s-s'); \quad \langle b_{in}^*(s)b_{in}(s') \rangle \\ &= [N(\omega_\omega)]\delta(s-s'),\end{aligned}\quad (8)$$

where  $N(\omega) = [\exp(\omega/k_B T) - 1]^{-1}$  and  $k_B$  and  $T$  stand for Boltzmann's constant and the operation temperature,

in the form of linearization approximations as

$$\begin{aligned}\dot{\delta a} &= -(i\Delta_c + \kappa_c)\delta a + iq_{OC}(|\beta|^2\delta a + \beta\alpha\delta b^+ + \beta^*\alpha\delta b) \\ &\quad + \sqrt{2\kappa_c}\delta a_{in}, \\ \dot{\delta b} &= -(i\Delta_\omega + \kappa_\omega)\delta b + iq_{OC}(|\alpha|^2\delta b + \beta\alpha\delta a^+ + \beta\alpha^*\delta a) \\ &\quad + \sqrt{2\kappa_\omega}\delta b_{in},\end{aligned}\quad (4)$$

where  $\alpha = \langle a \rangle$  and  $\beta = \langle b \rangle$  are the OC and MW cavity average modes, respectively. These parameters are calculated through the steady-state equations introduced as

$$\begin{aligned}-(i\Delta_c + \kappa_c)\alpha + iq_{OC}\alpha|\beta|^2 + E_c &= 0, \\ -(i\Delta_\omega + \kappa_\omega)\beta + iq_{OC}\beta|\alpha|^2 + E_\omega &= 0.\end{aligned}\quad (5)$$

Moreover, it is assumed that  $|\alpha|$  and  $|\beta| \gg 1$  [13]; hence,  $\alpha$  and  $\beta$  are approximated as

$$\alpha = \frac{E_c}{\kappa_c + i(\Delta_c - q_{OC}|\beta|^2)}, \quad \beta = \frac{E_\omega}{\kappa_\omega + i(\Delta_\omega - q_{OC}|\alpha|^2)}. \quad (6)$$

By calculating  $\alpha$  and  $\beta$  as the expectation values of the OC and MW cavity modes, respectively, Eq. (4) is solved. To study the entanglement between the modes of the cavities, one needs to use quadrature fluctuation, thus it is necessary to calculate their complex conjugates as  $\delta a^+$  and  $\delta b^+$ . Finally, the general form of Eq. (4), considering the operator's conjugates, is rewritten as

respectively [9,11]. Indeed,  $N(\omega)$  is the equilibrium mean thermal photon numbers of the different modes. It should be noted that the quantum noise source is deliberately neglected (i.e., shot noise [25] and 1/f noise [26]), because these noises are generally negligible compared with the thermal noise at high band-width operation [25]. In the simulation part, a GaAs photodetector is typically considered [27] and its bandwidth is usually assumed to be around  $B = 10$  GHz. This means 1/f noise can be completely ignored by considering such a high bandwidth. Therefore, in the following, particular emphasis is given to the quantum noise arising due to the quantization. When

a photodetector is utilized, it senses the incoming signal in the form of the quantized photons, and this leads to occurrence of the quantum noise and the related current fluctuation. During the random detection of the discrete particles, the rates of the detected particles fluctuate. It has been reported that the number of arriving discrete photons in a typical length of time ( $t_d$ ) is distributed according to the Poisson distribution [25]. So, after estimation of the probability of  $n$  arrival photons  $P_n(t)$ , the photon average number  $\langle n \rangle$ , and fluctuation  $\langle \delta n^2 \rangle$ , one can calculate the current “ $i$ ” and its fluctuation  $\langle \delta i^2 \rangle$  as [25]

$$\begin{aligned} i &= \frac{q}{t_d} n \longrightarrow I = \frac{q}{t_d} \langle n \rangle, \\ \langle \delta i^2 \rangle &= \frac{q^2}{t_d^2} \langle \delta n^2 \rangle \xrightarrow{\delta n = \langle n \rangle} = \frac{q}{t_d} I \xrightarrow{t_d = 1/2B} \langle \delta i^2 \rangle \\ &= 2qIB, \end{aligned} \quad (9)$$

where  $q$  is the electron charge,  $B$  is the photodetector bandwidth, and  $I$  is the average current  $I = \langle i \rangle$ . Another important parameter that should be considered in Eq. (10) is the photodetector quantum efficiency  $\zeta$ . Every received discrete photon has a probability  $\zeta$  of releasing either an electron or creating an electron-hole pair. Hence, the current fluctuation in Eq. (9) is rewritten as [25]

$$\langle \delta i^2 \rangle = 2q\zeta B \left( \frac{qP_c}{\hbar\omega_c} \right), \quad (10)$$

$$\begin{aligned} A &= \begin{bmatrix} \langle X_1^2 \rangle - \langle X_1 \rangle^2 \\ 0.5 \times \langle X_1 P_1 + P_1 X_1 \rangle - \langle X_1 \rangle \langle P_1 \rangle \end{bmatrix}, \\ B &= \begin{bmatrix} \langle X_2^2 \rangle - \langle X_2 \rangle^2 \\ 0.5 \times \langle P_2 X_2 + X_2 P_2 \rangle - \langle P_2 \rangle \langle X_2 \rangle \end{bmatrix}, \\ C &= \begin{bmatrix} 0.5 \times \langle X_1 X_2 + X_2 X_1 \rangle - \langle X_1 \rangle \langle X_2 \rangle \\ 0.5 \times \langle P_1 X_2 + X_2 P_1 \rangle - \langle P_1 \rangle \langle X_2 \rangle \end{bmatrix}, \end{aligned}$$

where  $X_1$ ,  $X_2$ ,  $P_1$ , and  $P_2$  are the quadrature fluctuations of the related modes. It should be noted that Eq. (11) is an important criterion for identification of the entanglement between two modes. Based on Eq. (11), it has been found that if  $2\eta > 1$ , the considered modes are purely separable; otherwise, for  $2\eta < 1$ , the two modes remain entangled [12]. However, one can use the Peres-Horodecki criterion for continuous state separability presented [11,28,29] as

$$\begin{aligned} \lambda_{\text{simon}} &= \det(A) \cdot \det(B) + (0.25 - |\det(C)|)^2 \\ &\quad - \text{tr}(AJCJB^TC^TJ) - 0.25 \times [\det(A) + \det(B)] \\ &\geq 0, \end{aligned} \quad (13)$$

where  $P_c/\hbar\omega_{\text{OC}}$  is the rate of the discrete arriving photons. However, it will be shown that the fluctuation of the current amplitude related to the shot noise is of the order of pA, whereas the photocurrent amplitude is of the order of  $\mu\text{A}$ . Due to this fact, the effect of the shot noise and the  $1/f$  noise is ignored in the calculation of the correlation matrix elements. This point will be evaluated in the result and discussion section in detail. The optoelectronic system stability is another interesting point to study in detail. Therefore, the matrix’s ( $A_{ij}$ ) eigenvalues are examined and it is shown that all of the real parts of the contributed eigenvalues are negative, indicating that the system operates in a stable state [13,14]. Hence, the quantum features of this system are analyzed. Since the tendency is toward entanglement between the modes in the designed system, the entanglement of the OC–MW cavity modes is especially examined. Considering the works published in the area, for measuring two-mode entanglement using Peres-Horodecki criterion [11], one can define a two-mode Gaussian state characterized by the corresponding correlation matrix elements. Thus, such a bipartite entanglement is quantified through the Symplectic eigenvalue introduced as [11,12,28]

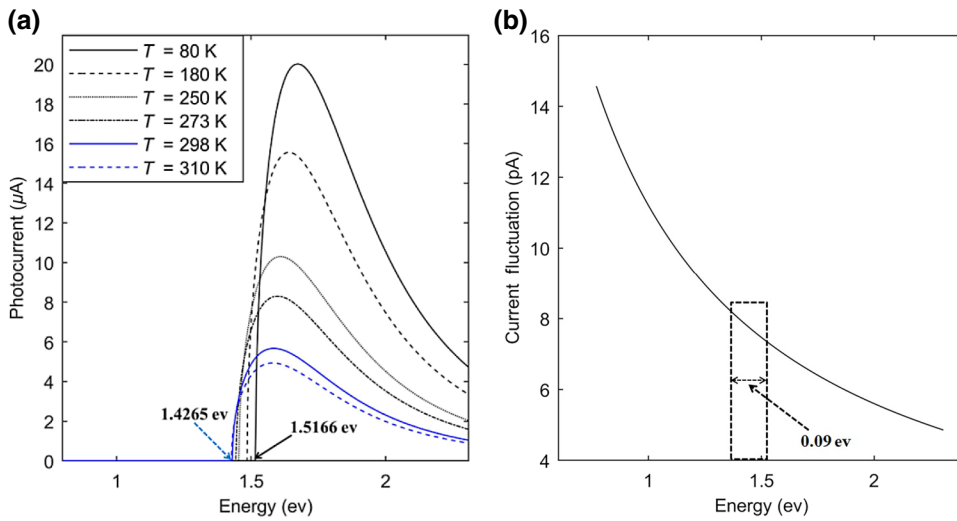
$$\eta = \frac{1}{\sqrt{2}} \sqrt{\sigma \pm \sqrt{\sigma^2 - 2 \det(\sigma)}}, \quad (11)$$

where  $\sigma = \det(A) + \det(B) - 2\det(C)$ , and “ $\det(:)$ ” indicates the determinant of the related matrix. In addition,  $A$ ,  $B$ , and  $C$  are  $2 \times 2$  correlation matrix elements [ $A$ ,  $C$ ;  $C^T$ ,  $B$ ], which can be expanded as

$$\begin{aligned} A &= \begin{bmatrix} 0.5 \times \langle X_1 P_1 + P_1 X_1 \rangle - \langle X_1 \rangle \langle P_1 \rangle \\ \langle P_1^2 \rangle - \langle P_1 \rangle^2 \end{bmatrix}, \\ B &= \begin{bmatrix} 0.5 \times \langle X_2 P_2 + P_2 X_2 \rangle - \langle X_2 \rangle \langle P_2 \rangle \\ \langle P_2^2 \rangle - \langle P_2 \rangle^2 \end{bmatrix}, \\ C &= \begin{bmatrix} 0.5 \times \langle X_1 P_2 + P_2 X_1 \rangle - \langle X_1 \rangle \langle P_2 \rangle \\ 0.5 \times \langle P_1 P_2 + P_2 P_1 \rangle - \langle P_1 \rangle \langle P_2 \rangle \end{bmatrix}, \end{aligned} \quad (12)$$

where  $J = [0, 1; -1, 0]$ . The Peres-Horodecki criterion in Eq. (13) is a necessary and sufficient condition for separability for all bipartite Gaussian states systems. To understand how entanglement is actually computed in this work, and how the correlation matrix elements ( $A$ ,  $B$ , and  $C$ ) are calculated, one can find sufficient details in the Appendix [11,28–30].

In this study, this criterion is applied to determine whether the considered modes are entangled. In the next section, the OC and MW cavity coupling factor ( $q_{\text{OC}}$ ) is derived. In fact, it is an important factor by which one can control the coupling between two cavity modes and eventually examine the entanglement between the modes.



Determining the factor,  $q_{\text{OC}}$ , leads to generating the photocurrent through coupling of the OC mode to the photodiode ( $f_1$ ). Then the photocurrent is found to strongly influence the voltage across the Varactor diode ( $f_2$ ). Thus, the MW cavity specifications are also affected by  $f_2$ .

### C. Photocurrent calculation using the time-dependent perturbation theory

To calculate the current through the photodetector due to the incidence wave, the time-dependent perturbation theory is employed. This is used because the incident light amplitude on the materials is relatively weak compared to the fields within the materials. With this theory, the wave function at some later time is calculated. Accordingly, the system Hamiltonian is expressed as  $H = H_0 + H_{\text{int}}(t)$ . To deal with such a situation, the time-dependent Schrödinger equation  $i\hbar d|\Psi\rangle/dt = H|\Psi\rangle$  is used, where  $|\Psi\rangle$  is the time-varying wave vector.  $|\Psi_n\rangle$  and  $E_n$  are assumed as the eigenfunction and eigenvalue of the time-independent equation ( $H_0|\Psi_n\rangle = E_n|\Psi_n\rangle$ ). Therefore, one can expand the solution of the time-dependent equation as  $|\Psi\rangle = \{\sum_n a(t) \exp[-iE_n t/\hbar]\} |\Psi_n\rangle$ . By substituting  $|\Psi\rangle$  into the time-dependent Schrödinger equation and premultiplying in  $\langle\Psi_q|$ , and by considering the perturbation series, the first-order eigen function [31,32] is obtained as

$$\begin{aligned} \dot{a}_q^{(1)}(t) &= \frac{1}{i\hbar} \cdot \sum_n a_n^{(0)}(t) \cdot e^{i\omega_{qn}t} \langle \Psi_q | H_{\text{int}}(t) | \Psi_n \rangle, \quad \omega_{qn} \\ &= \frac{E_q - E_n}{\hbar}, \end{aligned} \quad (14)$$

where  $|\Psi_n\rangle$  is the initial state and  $|\Psi_q\rangle$  is the state in which we are interested (a favorite state). To solve Eq. (14), one should know the perturbing Hamiltonian of the designed system. For the sake of simplicity, the perturbing Hamiltonian is semiclassically defined as

FIG. 2. (a) Photocurrent ( $\mu\text{A}$ ) vs incident wave energy (ev) at different temperatures; (b) Photocurrent fluctuation (pA) vs incident wave energy (ev);  $P_c = P_w = 10 \text{ mW}$ .

$H_{\text{int}}(t) = -q.E(t)$ . Hence, by substituting the interaction Hamiltonian into Eq. (14) and also with an additional assumption that the perturbation starts at  $t = 0$  and ends at  $t = t_0$ ,  $a_q^{(1)}(t)$  is given by

$$\begin{aligned} a_q^{(1)}(t) &= \frac{1}{i\hbar} \cdot \int_0^{t_0} e^{i\omega_{qn}t} \langle \Psi_q | H_{\text{int}}(t) | \Psi_g \rangle dt \\ &= \frac{1}{i\hbar} \cdot \langle \Psi_q | H_{\text{int}0} | \Psi_g \rangle \int_0^{t_0} e^{i[\omega_{qn}-\omega]t} \\ &\quad + e^{i[\omega_{qn}+\omega]t} dt. \end{aligned} \quad (15)$$

In this study, the OC modes coupling to the photodiode, being proportional to the absorption rate is examined. Thus, from Eq. (15), the total rate of the transition in the presence of the OC electric field is given by

$$q_{\text{OC}} = \frac{2\pi}{\hbar} \cdot |\langle \Psi_q | H_{\text{int}0} | \Psi_g \rangle|^2 L(\omega_{qg}) \cdot g_J(\hbar\omega_{qg}), \quad (16)$$

where  $L(\omega_{qg})$  is the Lorentzian function. In fact, this function is utilized because no line becomes arbitrarily sharp, suggesting that the contributed energy is well defined. Therefore, a very dense transition as  $g_J(\omega_{qg})$  is defined for this purpose. By considering the interaction Hamiltonian and using Fermi's Golden rule [33,34], the coupling factor, or the total transition rate, is given by

$$\begin{aligned} q_{\text{OC}} &= \frac{2\pi}{\hbar} \cdot \frac{e^2 A_0^2}{4m_0^2} \cdot |P_{cv}|^2 \cdot \frac{1}{2\pi^2} \cdot \left( \frac{2\mu_{\text{eff}}}{\hbar^2} \right)^{1.5} \\ &\quad \cdot \sqrt{\hbar\omega_c - E_{\text{gap}}(T)L(\omega_{eg})} \cdot f(T), \end{aligned} \quad (17)$$

where  $e$ ,  $m_0$ ,  $A_0^2$ , and  $P_{cv}$  are, respectively, the electron charge, the free electron mass, the optical intensity, and the matrix element that equals  $\langle c|\mathbf{P}|v\rangle$ , where  $c$  and  $v$  denote

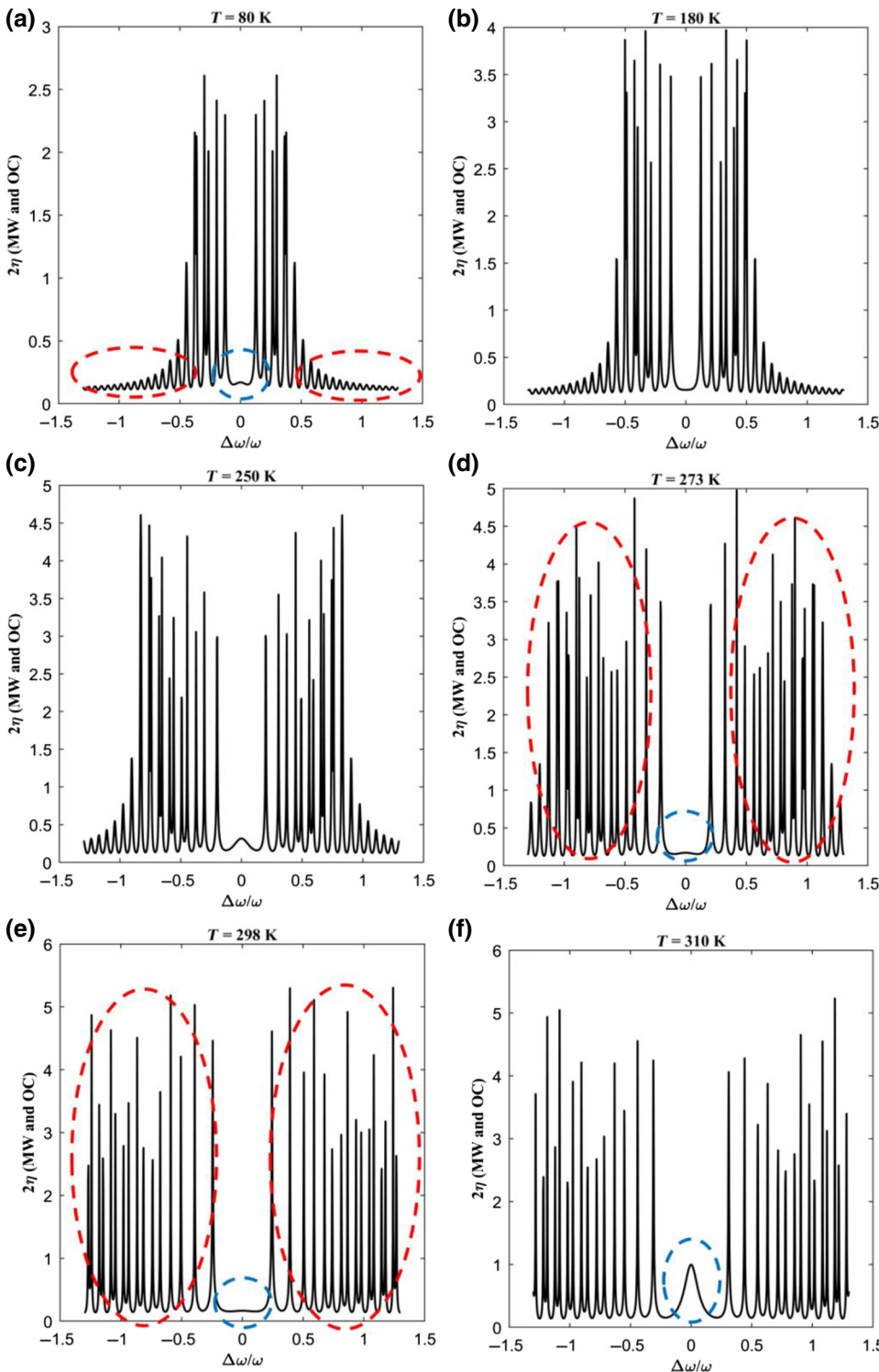


FIG. 3. Entanglement analysis for two (MW and OC) cavity modes vs  $\Delta\omega/\omega$  at  $\Delta c = 0$  at different temperatures, (a) 80 K, (b) 180 K, (c) 250 K, (d) 273 K, (e) 298 K, and (f) 310 K.  $P_c = P_w = 10$  mW.

the conduction and valence bands.  $\mu_{\text{eff}}$  is the electron-hole effective mass. More importantly,  $f(T)$  is the temperature factor that depends on the (i) thermal distribution of the electrons in the excited and ground states and (ii) relaxation time from the photo-excited state to other states. Generally, the function,  $f(T)$ , is the main reason for the strong dependence of the photocurrent on the operational

temperature. This means that at higher temperatures, the photocurrent is dramatically decreased [35,36]. Finally,  $E_{\text{gap}}(T)$  is the photodetector energy band gap known to be dependent on temperature. It has been shown that the band-gap energy is influenced by the generated phonons [37,38]. A few useful approaches such as the Varshni relation have been suggested [38] in which the band gap of the

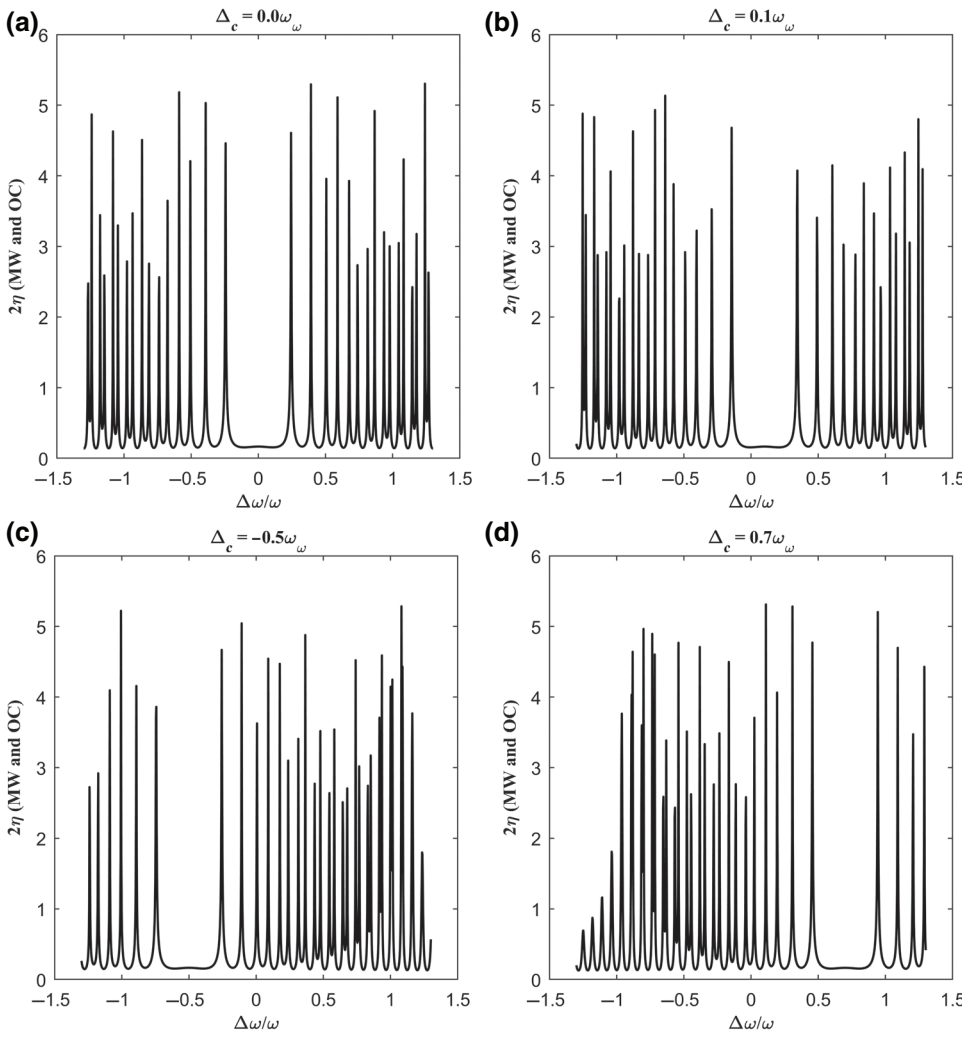


FIG. 4. Entanglement analysis for two (MW and OC) cavity modes vs  $\Delta\omega/\omega$  at different  $\Delta_c$ , (a)  $\Delta_c = 0\omega_\omega$ , (b)  $\Delta_c = 0.1\omega_\omega$ , (c)  $\Delta_c = -0.5\omega_\omega$ , (d)  $\Delta_c = 0.7\omega_\omega$ .  $T = 298 \text{ K}$ ,  $P_c = P_w = 10 \text{ mW}$ .

semiconductor is fitted by some of the parameters' characteristics of a considered material. However, in this study, Eq. (18) is employed [37]

$$E_{\text{gap}}(T) = E_{\text{gap}0} - S < \hbar\omega_{\text{phonon}} \\ > [\coth(\langle \hbar\omega_{\text{phonon}} \rangle / 2kT) - 1], \quad (18)$$

where  $E_{\text{gap}0}$ ,  $S$ , and  $\langle \hbar\omega_{\text{phonon}} \rangle$  are the material band gap at zero temperature, the coupling constant, and the average phonon energy, respectively. To simplify, the effect of the thermal photon on the band-gap broadening is ignored. This is due to the fact that the system used in this study does not contain any mechanical parts, so the generated thermal photons are dramatically decreased. Parameters fitted for the temperature dependence of the band gap in Eq. (18) are taken from [37]. Equation (17) introduces the total transition rate, which is the actual coupling parameter between the OC and MW cavity modes. Indeed,  $q_{\text{OC}}$  is a sole parameter that can be used to control the OC and MW

cavity modes' coupling. It is emphasized that  $q_{\text{OC}}$  is dramatically affected by the OC mode's frequency and also by the ambient temperature.

### III. RESULTS AND DISCUSSION

Due to the role of the transition rate factor in the coupling between cavity modes and its effect on the quantum features of the related modes, the parameters that influence the photocurrent and its fluctuation are investigated in this study. It is supposed that this photodetector is a direct band-gap GaAs photodetector with an energy band gap of around  $E_{\text{gap}0} = 1.52 \text{ eV}$ . Hence, by sweeping the incoming light frequencies  $\omega_{\text{OC}}$ , the amount of the generated photocurrent is estimated [Fig. 2(a)]. It should be noted that by increasing the temperature, the amplitude of the photocurrent due to the thermal noise effect is decreased. Moreover, the maximum amplitude for each chart in the figure occurs where the OC mode incident frequency is close to the band-gap energy. From Eq. (18), it is clearly observable that the considered photodetector band gap is dependent

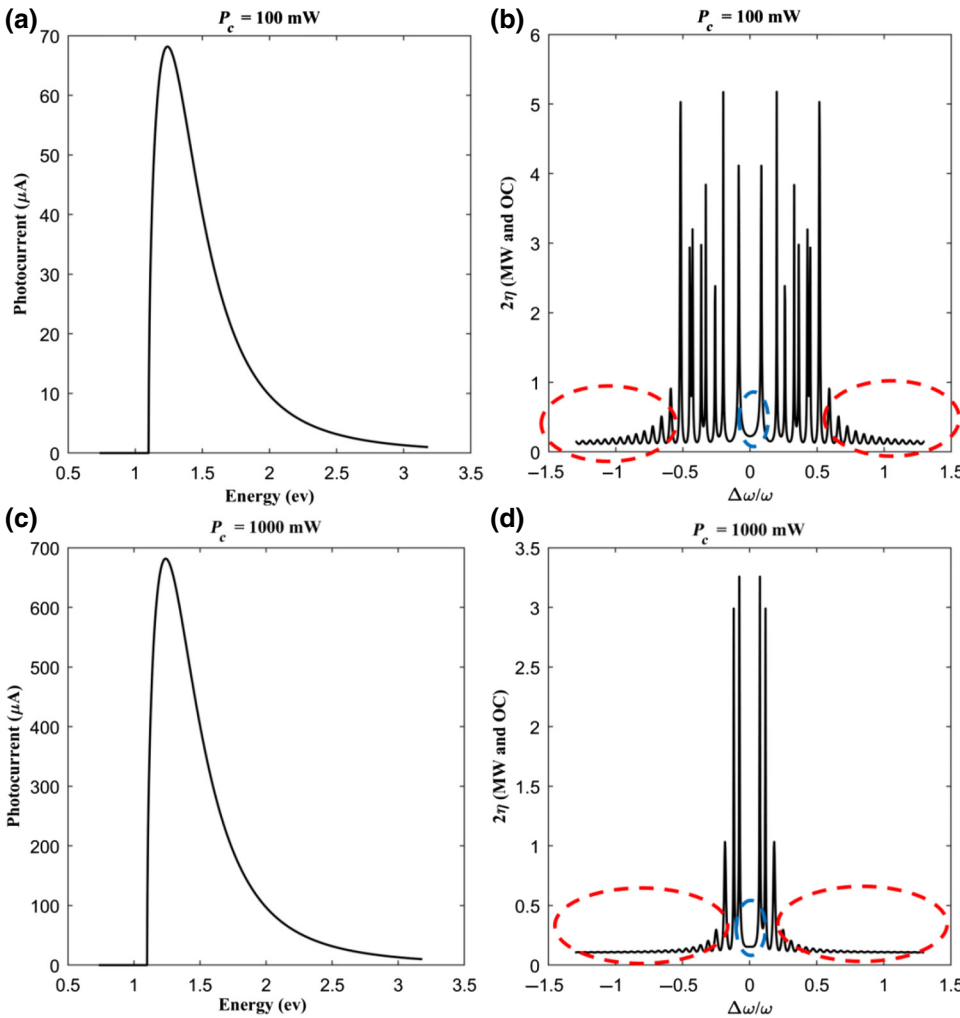


FIG. 5. The effect of the optical cavity pumping on the photocurrent (lefthanded) and entanglement between two modes (right handed) at different optical cavity pumping; (a),(b)  $P_c = 100 \text{ mW}$ , (c),(d)  $P_c = 1000 \text{ mW}$ .  $T = 298 \text{ K}$ ,  $\Delta_c = 0.0\omega_\omega$ ,  $P_w = 10 \text{ mW}$ .

on the temperature; accordingly, in this figure, it is shown that by increasing the temperature from 80 to 310 K, the actual band gap is decreased from 1.5166 to 1.4265 eV. The decreasing range of the band-gap energy due to the temperature increase is around  $\Delta E = 0.09$  eV, which is not sufficiently high to influence the system's operation. Moreover, the photocurrent fluctuation is simulated based on Eq. (10) and the result is depicted in Fig. 2(b). It is shown that the amplitude of the current fluctuation is very small, 8 pA, compared to the photocurrent average, 10  $\mu\text{A}$ . Moreover, for better illustration of the changing of the current fluctuation within the band-gap energy variation, a dashed rectangle is attached in Fig. 2(b). Therefore, the simulated data suggests that the quantum noise effect is negligible. Furthermore, the dark current effect, for simplicity, is neglected.

The results of the optoelectronic circuit parameters influencing the entanglement between the OC and MW cavity modes are illustrated in Fig. 3. Generally, it is known that by increasing the system's temperature, the entanglement between the two modes should be decreased.

Thus, one can compare the amplitude of the subfigures in Fig. 3. It is shown that by increasing the temperature, the amplitude of  $2\eta$  is generally increased, meaning that the separability between the cavity modes is increased. However, it is also observed that the latter expression is valid for every MW cavity detuning frequency  $\Delta\omega/\omega$  (shown with a red-dashed circle) except  $\Delta\omega/\omega \sim 0$ . For better understanding, one can compare the red-dashed ellipsoid in the subfigures. For instance, the comparison between Fig. 3(a) and Fig. 3(e) reveals that at  $T = 80 \text{ K}$ , for many cavity detuning frequencies, the two cavity modes remain entangled. Whereas at  $T = 298 \text{ K}$ , the modes' entanglement is dramatically reduced, which is strongly related to the thermal photon generation.

Moreover, the important point is that the divergence slopes at each profile are intensified with the increasing temperature. As a matter of fact, an interesting event is observed around  $\Delta\omega/\omega \sim 0$ , which is marked with the blue-dashed circle on a few figures. In this regard, it is shown that by increasing the temperature up to 300 K, the two considered modes remain entangled. This result is the

most important achievement obtained in this study. In our previous work [17], it was theoretically shown that the cavity modes' entanglement at room temperature is not accessible by a plasmonic optomechanical system. Furthermore, in Fig. 3(f), when the temperature is increased to 310 K, at  $\Delta_\omega/\omega = 0$ , entanglements start declining; however,  $2\eta$  remains smaller than unity, indicating the entanglement is still evident. It can be briefly deduced that using the optoelectronic system rather than the optomechanical system helps to reduce the system's thermal-induced noise, so the entangled modes are easily accessible at room temperature. In other words, utilizing the optoelectronic element as a coupler between the OC and MW cavities leads to a decline in the generation of the thermal photons, which strongly disturbs the system's operation. Meanwhile, the mechanical element in the optomechanical system is an original source for introducing the thermal photon noise into a system. Considering the knowledge about the advantages of an optoelectronic system, one can briefly deduce that this type of system seems to be the best option for the replacement of the optomechanical part in a quantum illumination system.

Another interesting investigation of this study concerns the engineering of the entanglement area observed in the vicinity of  $\Delta_\omega/\omega \sim 0$ , shown with the dashed-blue circle in Fig. 3. The new investigation results are shown in Fig. 4. This figure reveals that the entanglement between modes for different detuning factors  $\Delta_c$  is found at points where  $\Delta_c = \Delta_\omega$ . Therefore, by adjusting the detuning factor, the region where the two modes are fully entangled is established. To our knowledge, this point can be considered as a degree of freedom in quantum properties or more specifically in the entanglement engineering. From these simulations, it can be briefly concluded that by controlling the OC modes' coupling to the photodiode, the flowing current is altered, thus the Varactor diode-biased voltage is mutually changed, and eventually, the MW cavity modes are affected. In fact, by controlling the photocurrent, the coupled modes' entanglement will be engineered.

Another method for manipulating the entanglement between modes is varying the OC pumping amplitude ( $P_c$ ). In fact, this is the case that directly affects the Varactor diode's biasing voltage, and then the MW cavity mode is changed. For this reason, a few simulations are carried out in which the effect of changing the OC pumping amplitude is considered. Initially, the effect of  $P_c$  on the photocurrent amplitude is studied. It is clear that by increasing the OC driving power, the generated current amplitude  $A_c$  is increased. To understand the situation better, one should compare Figs. 5(a) and 5(c), even though it is theoretically proved by Eq. (17). At a quick glance, it is comprehensible that by increasing  $P_c$ , the amplitude of the  $2\eta$  generally decreases, meaning that by increasing the coupling factor, the modes are going to be strongly entangled. Comparing

Fig. 3(e) with Figs. 5(b) and 5(d) reveals that the amount of divergence in the entanglement profile for different  $\Delta_\omega$  is dramatically reduced. This is explained in that increasing  $P_c$  leads to intensifying the total transition rate [Fig. 5(c)]. The entanglement between the related modes is broadened by increasing the coupling factor for the case of different  $\Delta_\omega$  (red-dashed line). Accordingly, as an interesting conclusion of this work, it is shown that the entanglement at  $\Delta_\omega = 0$  is not affected by any parameters (blue-dashed line) at room temperature.

The above results show that removing the mechanical part of the traditional tripartite system [13–17] does not have any catastrophic effects on the system performance, such as OC and MW cavity modes' entanglement and dynamics equations' stability [13,14]. Instead, it is shown that removing the mechanical part leads to strongly decreasing the system complexity, simplifying the analyzing approach, and more importantly, the design without the mechanical part operates safely at room temperature. The latter case, which is an important feature of this study, strongly contributes to decreasing the thermal photons generated in the system. The thermal photons' noise is largely generated due to the low-frequency operation of the mechanical part in traditional tripartite systems. Therefore, due to the reasons mentioned in this work, through bypassing the mechanical parts, the photodetector together with the Varactor diode directly couple the OC mode to the MW cavity mode with no need for any mechanical parts.

#### IV. CONCLUSIONS

In this article, an alternative optoelectronics system is designed for direct coupling of the OC and MW cavity modes. One of the major aims of this study is to investigate the entanglement between the OC and MW cavity modes. For this reason, the dynamics of the motion of the designed system is analyzed with Heisenberg-Langevin equations. The main question is how the photocurrent created as a function of the OC mode coupling to the MW cavity modes manipulates the characteristics. Accordingly, the photocurrent is affected by the voltage developed across the Varactor diode, suggesting that the Varactor internal capacitance is directly dependent on the photocurrent. Also in this study, the details of coupling between the OC and MW cavity modes are investigated. Finally, the entanglement between the OC and MW cavity modes is theoretically analyzed, and the results indicate that the two modes can be entangled at room temperature. It is also shown that the classical optomechanical systems can be replaced by the optoelectronic system proposed in this study. The optoelectronic system design provides a degree of freedom to control the thermally generated photons to maintain entanglement and also to

allow simplifying the complexities due to the mechanical elements.

## APPENDIX

We briefly present a two-mode entanglement criterion introduced by Simon [11]. This criterion is based upon the negativity of partial transposes of a bipartite system and is a necessary and sufficient condition for a Gaussian state [11,28,29]. A Gaussian state is a more important and simple class of continuous variable systems and is characterized as a state whose Wigner function (quasiprobability distribution) is a Gaussian state [29]. It is a popular method because using the Wigner distribution, the quantum operators are related to their corresponding phase space variables [30]. It has been shown that the system's density matrix (quantum ensembles) is a Gaussian state when it is presented as a form of the Wigner distribution for a single-mode coherently squeezed (or coherent) state. Hence, information only about the mean and variance are sufficient to describe this system's state. Therefore, we are ready to apply the separability criterion proposed by Simon [11], which is basically a generalization of the Peres-Horodecki criterion for two-mode entanglement measuring. Generally, bipartite (two-mode) separable states can be expressed in terms of a summation of tensor products

between the two subsystems' density matrices, which is given by

$$\rho = \sum_j P_j \rho_1^j \otimes \rho_2^j \quad (\text{A1})$$

where  $\rho_1$ ,  $\rho_2$ , and  $P_j$  are the subsystem's density matrices and probability, respectively. An entangled state is a state that cannot be presented in the form of Eq. (A1) and the subsystems' behaviors correlate to each other in a nontrivial fashion. In the following, for two-mode entanglement measured by the Peres-Horodecki criterion, we define a two-mode Gaussian state, which can be completely characterized by its corresponding correlation matrix elements as

$$\begin{aligned} V_{ij} &= \frac{1}{2} \langle \hat{Y}_i \hat{Y}_j + \hat{Y}_j \hat{Y}_i \rangle - \langle \hat{Y}_i \rangle \langle \hat{Y}_j \rangle, Y \\ &= [\hat{x}_1, \hat{p}_1, \hat{x}_2, \hat{p}_2], \hat{x}_{i\_out} = (a_{i\_out} + a_{i\_out}^\dagger), \hat{p}_{i\_out} \\ &= 1/i\sqrt{2}(a_{i\_out} - a_{i\_out}^\dagger) \end{aligned} \quad (\text{A2})$$

After calculation of the correlation matrix  $V_{4 \times 4} = [A, C; C^T, B]$  the two-output modes' separability measurements are analyzed. In this equation,  $A$ ,  $B$ , and  $C$  are  $2 \times 2$  matrixes whose elements are calculated from  $V_{ij}$  as

$$\begin{aligned} A &= \begin{bmatrix} \langle X_1^2 \rangle - \langle X_1 \rangle^2 & 0.5 \times \langle X_1 P_1 + P_1 X_1 \rangle - \langle X_1 \rangle \langle P_1 \rangle \\ 0.5 \times \langle X_1 P_1 + P_1 X_1 \rangle - \langle X_1 \rangle \langle P_1 \rangle & \langle P_1^2 \rangle - \langle P_1 \rangle^2 \end{bmatrix}, \\ B &= \begin{bmatrix} \langle X_2^2 \rangle - \langle X_2 \rangle^2 & 0.5 \times \langle X_2 P_2 + P_2 X_2 \rangle - \langle X_2 \rangle \langle P_2 \rangle \\ 0.5 \times \langle X_2 P_2 + P_2 X_2 \rangle - \langle X_2 \rangle \langle P_2 \rangle & \langle P_2^2 \rangle - \langle P_2 \rangle^2 \end{bmatrix}, \\ C &= \begin{bmatrix} 0.5 \times \langle X_1 X_2 + X_2 X_1 \rangle - \langle X_1 \rangle \langle X_2 \rangle & 0.5 \times \langle X_1 P_2 + P_2 X_1 \rangle - \langle X_1 \rangle \langle P_2 \rangle \\ 0.5 \times \langle X_1 P_2 + P_2 X_1 \rangle - \langle X_1 \rangle \langle P_2 \rangle & 0.5 \times \langle P_1 P_2 + P_2 P_1 \rangle - \langle P_1 \rangle \langle P_2 \rangle \end{bmatrix}. \end{aligned} \quad (\text{A3})$$

Finally, the exact form of the Peres-Horodecki criterion for continuous state separability presented by Simon [11,28] is introduced as

$$\begin{aligned} \lambda_{\text{simon}} &= \det(A) \cdot \det(B) + (0.25 - |\det(C)|)^2 \\ &\quad - \text{tr}(AJCJB^TC^TJ) - 0.25 \times (\det(A) + \det(B)) \\ &\geq 0, \end{aligned} \quad (\text{A4})$$

where  $J = [0, 1; -1, 0]$ . The Peres-Horodecki criterion in Eq. (A4) is a necessary and sufficient condition for separability for all bipartite Gaussian state systems. In this article, for simplicity, we call this criterion the “Simon criterion.”

Furthermore, two-mode entanglement can be measured by considering the Symplectic eigenvalue calculation, which is given by [28].

$$\begin{aligned} \eta &= 1/\sqrt{2} \times \sqrt{\sigma(V) - \sqrt{\sigma(V) - 4 \det(\sigma(V))}}, \quad \sigma(V) \\ &= \det(A) + \det(B) - 2 \det(C). \end{aligned} \quad (\text{A5})$$

[1] Y. Shih, Quantum imaging, *IEEE J. Sel. Top. Quantum Electron.* **13**, 1016 (2007).

- [2] A. Salmanoglu, H. S. Geçim, and E. Bişkin, Plasmonic system as a compound eye: Image point-spread function enhancing by entanglement, *IEEE Sens. J.* **18**, 5723 (2018).
- [3] M. Lanzagorta, Quantum Radar, *Synth. Lect. Quantum Comput.* **3**, 1 (2012).
- [4] S. Lloyd, Enhanced sensitivity of photodetection via quantum illumination, *Science* **321**, 1463 (2008).
- [5] Y. Shih, Entangled photons, *IEEE J. Sel. Top. Quantum Electron.* **9**, 1455 (2003).
- [6] M. H. Rubin, D. N. Klyshko, Y. H. Shih, and A. V. Sergienko, Theory of two-photon entanglement in type-II optical parametric down-conversion, *Phys. Rev. A* **50**, 1050 (1994).
- [7] Y. Shih, Entangled biphoton source—property and preparation, *Rep. Prog. Phys.* **66**, 1009 (2003).
- [8] A. Salmanoglu and H. S. Geçim, Array of nanoparticles coupling with quantum-dot: Lattice plasmon quantum features, *Physica E* **100**, 54 (2018).
- [9] A. Salmanoglu and H. S. Geçim, Quantum eye: Lattice plasmon effect on quantum fluctuation and photon detection, *Ann. Phys.* **394**, 162 (2018).
- [10] A. Salmanoglu, Raman modes non-classicality through entangled photons coupling to plasmonic modes, *J. Opt. Soc. Am. B* **35**, 2467 (2018).
- [11] R. Simon, Peres-Horodecki Separability Criterion for Continuous Variable System, *Phys. Rev. Lett.* **84**, 2726 (2000).
- [12] W. Ge, M. E. Tasgin, and M. S. Zubairy, Conservation relation of nonclassicality and entanglement for Gaussian states in a beam splitter, *Phys. Rev. A* **92**, 052328 (2015).
- [13] Sh. Barzanjeh, D. Vitali, P. Tombesi, and G. J. Milburn, Entangling optical and microwave cavity modes by means of a nanomechanical resonator, *Phys. Rev. A* **84**, 042342 (2011).
- [14] N. Aggarwal, K. Debnath, S. Mahajan, A. B. Bhattachjee, and Man Mohan, Selective entanglement in a two-mode optomechanical system, arXiv.org > quant-ph > arXiv:1404.6712v1 (2014).
- [15] C. Genes, A. Mari, P. Tombesi, and D. Vitali, Robust entanglement of a micromechanical resonator with output optical fields, *Phys. Rev. A* **78**, 032316 (2008).
- [16] D. Vitali, S. Gigan, A. Ferreira, H. R. Bohm, P. Tombesi, A. Guerreiro, V. Vedral, A. Zeilinger, and M. Aspelmeyer, Optomechanical Entanglement between a Movable Mirror and a Cavity Field, *Phys. Rev. Lett.* **98**, 030405 (2007).
- [17] A. Salmanoglu and H. S. Geçim, Optical and Microcavity Modes Entanglement by means of Developed Opto-Mechanical System, arXiv:1804.11183 [quant-ph] (2018).
- [18] G. Konstantatos and E. H. Sargent, Colloidal quantum dot photodetector, *Infrared Phys. Technol.* **54**, 278 (2011).
- [19] D. C. Oertel and M. G. Bawendi, Photodetectors based on treated CdSe quantum-dot films, *Appl. Phys. Lett.* **87**, 213505 (2005).
- [20] G. Konstantatos, J. Clifford, L. Levina, and E. H. Sargent, Sensitive solution-processed visible-wavelength photodetectors, *Nat. Photonics* **1**, 531 (2007).
- [21] F. J. Hyde, S. Deval, C. Toker, Varactor Diode Measurements, the Radio and Electronic Engineer, U.D.C. 621.382.232.3.011.4 67 (1966).
- [22] High Speed Photodetector GaAs Detector, technical data sheet, [www.neontech.cc/](http://www.neontech.cc/).
- [23] SMV1702-011LF Hyperabrupt Junction Tuning Varactor, technical Data sheet, Skyworks Solutions, Inc., [www.skyworksinc.com](http://www.skyworksinc.com).
- [24] B. Huttner and S. M. Barnett, Quantization of electromagnetic field in dielectrics, *Phys. Rev. A* **46**, 4306 (1992).
- [25] B. M. Oliver, Thermal and quantum noise, *Proc. IEEE* **53**, 436 (1965).
- [26] J. F. Valtueña, J. A. Garrido, and J. I. Izpura, 1/f noise in InGaAs/GaAs linear graded buffer layer, *IEEE Trans. Electron. Devices* **45**, 1201 (1998).
- [27] S. Y. Wang and D. M. Bloom, 100 GHz Bandwidth Planar GaAs Schottky Photodiode, *Electron. Lett.* **19**, 554 (1983).
- [28] M. E. Tasgin, Single-mode nonclassicality measure from Simon-Peres-Horodecki criterion, arXiv:quanta-ph/15020 0992v1 (2015).
- [29] R. Simon and E. C. G. Sudarshan, Gaussian-signer distributions in quantum mechanics and optics, *Phys. Rev. A* **36**, 3868 (1987).
- [30] T. Deesawan, *Entanglement Criteria for Continuous-Variable States* (Master of Science of Imperial College London, London, 2010).
- [31] E. Feenberg, A note on perturbation theory, *Phys. Rev.* **74**, 206 (1948).
- [32] F. J. Dvsox, Divergence of perturbation theory in quantum electrodynamics, *Phys. Rev.* **85**, 631 (1951).
- [33] L. B. Mendelsohn, High-order perturbation theory for a one-electron ion in a uniform electric field, *Phys. Rev.* **176**, 90 (1968).
- [34] M. Hillery, Fermi's golden rule and exponential decay in two-level systemse, *Phys. Rev. A* **24**, 933 (1981).
- [35] A. Asgari and S. Razi, High performances III-nitride quantum dot infrared photodetector operating at room temperature, *Opt. Express* **18**, 14604 (2010).
- [36] H. Lim, W. Zhang, S. Tsao, T. Sills, J. Szafraniec, K. Mi, B. Movaghfar, and M. Razeghi, Quantum dot infrared photodetectors: Comparison of experiment and theory, *Phys. Rev. B* **72**, 085332 (2005).
- [37] K. P. O' Donnell and X. Chen, Temperature dependence of semiconductor band gaps, *Appl. Phys. Lett.* **58**, 2924 (1991).
- [38] Y. P. Varshni, Temperature dependence of the energy gap in semiconductors, *Physica* **34**, 149 (1967).